Dissociation Kinetics of (*N*-Methylacetohydroxamato)iron(III) Complexes: A Model for Probing Electronic and Structural Effects in the Dissociation of Siderophore Complexes

M. Tyler Caudle and Alvin L. Crumbliss*

Department of Chemistry, Box 90346, Duke University, Durham, North Carolina 27708-0346

Received February 3, 1994®

The proton-initiated dissociation kinetics and equilibria of the mono, bis, and tris complexes of iron(III) with *N*-methylacetohydroxamic acid (NMHA) were studied under conditions of 2.0 M $NaClO_4/HClO_4$ at 25 °C. The proton-dependent rate constants k_3, k_2, and k_1 for dissociation of the tris, bis, and mono complexes are 8.6×10^3 M^{-1} s^{-1}, 1.02×10^2 M^{-1} s^{-1}, and 3.2×10^{-3} M^{-1} s^{-1}, respectively. The corresponding equilibrium constants log K_3, log K_2, and log K_1 are 1.06, –0.9, and –2.75, respectively. An acid-independent dissociation pathway is observed in the dissociation of the mono complex with a rate constant $k'_1 = 7.1 \times 10^{-3}$ s^{-1}. The solution NMR spectrum of the ligand shows split methyl peaks indicating hindered rotation about the C–N bond. The equilibrium ratio for the C–N rotation was found to be 3.5 in favor of the *Z* isomer and the minimum lifetime of the rotation was estimated to be 0.3 s. The rates and mechanism of $Fe(NMHA)_i^{3-i}$ dissociation are compared to corresponding processes observed for dissociation of (acetohydroxamato)iron(III) complexes and the natural trihydroxamate siderophore ferrioxamine B. Differences in rate and mechanism between the model systems and ferrioxamine B are discussed in terms of solvent effects, electrostatic effects, and C–N bond rotation in the hydroxamate group.

Introduction

Past and current interest in hydroxamic acids, or *N*-hydroxy amides, centers in large part around their profound iron binding properties.[1-10] The bidentate ligand can form extremely stable five-membered rings with iron(III), as illustrated in eq 1. In fact,

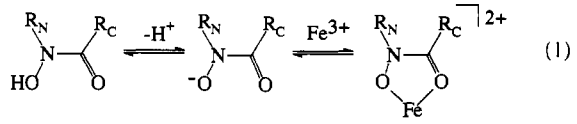

(1)

many microbial iron transport complexes, called siderophores, contain hydroxamate functional groups as the iron binding sites.[11-15] There are numerous studies involving synthetic hydroxamic acids as model iron binding siderophores.[11-15] In addition, a few hydroxamic acids have attracted clinical interest related to iron binding as iron chelators in the treatment of iron-overload disorders,[15-19] in the possible treatment of lung silicosis,[20,21] and as antimalarials[22,23] and antibacterials.[15,24,25] Also, some hydroxamic acids exhibit antitumor activity,[24] though it is not clear whether the mechanism for such activity is at all related to iron binding.

Monohydroxamic acids are believed to have the two resonance forms **Ia** and **Ib**.[7,8,26] Evidence for the presence of **Ia,b** comes

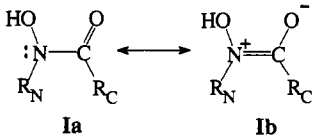

Ia **Ib**

from NMR data where hindered rotation about the C–N bond has been observed experimentally for acetohydroxamic acid (AHA, **I**, $R_N = H$, $R_C = CH_3$)[27] and, in this study, for *N*-methylacetohydroxamic acid (NHMA, **I**, $R_N = CH_3$, $R_C = CH_3$). In **Ib** there is a partial positive charge on the nitrogen that may be stabilized or destabilized by an electron-donating or -withdrawing substituent at that position. Since the electron density on the carbonyl oxygen is greater in **Ib** than in **Ia**,

* Author to whom correspondence should be addressed.

® Abstract published in *Advance ACS Abstracts,* July 1, 1994.

(1) Funahashi, S.; Koji, I.; Tanaka, M. *Inorg. Chem.* **1983**, *22*, 2070.
(2) Biruš, M.; van Eldik, R. *Inorg. Chem.* **1991**, *30*, 4559.
(3) Biruš, M.; Bradić, Z.; Kijundžić, N.; Pribanić, M.; Wilkins, P. C.; Wilkins, R. G. *Inorg. Chem.* **1985**, *24*, 3980.
(4) Chang, C. A.; Sekhar, V. C.; Garg, B. S.; Guziec, F. S.; Russo, T. C. *Inorg. Chima. Acta* **1987**, *135*, 11.
(5) Brown, D. A.; McKeith, D.; Glass, W. K. *Inorg. Chim. Acta* **1979**, *35*, 5.
(6) Biruš, M.; Kujundžić, N.; Pribanić, M. *Inorg. Chim. Acta* **1980**, *55*, 65.
(7) Monzyk, B.; Crumbliss, A. L. *J. Am. Chem. Soc.* **1979**, *101*, 6203.
(8) Brink, C. P.; Brumbliss, A. L. *Inorg. Chim.* **1984**, *23*, 4708.
(9) Monzyk, B.; Crumbliss, A. L. *J. Am. Chem. Soc.* **1982**, *104*, 4921.
(10) Biruš, M.; Bradić, Z.; Krznarić, G.; Kujundžić, N.; Pribanić, M.; Wilkins, P. C.; Wilkins, R. G. *Inorg. Chem.* **1987**, *26*, 1000.
(11) Raymond, K. N.; Müller, G.; Matzanke, B. F. *Top. Curr. Chem.* **1984**, *123*, 49.
(12) Crumbliss, A. L. In *CRC Handbook of Microbial Iron Chelates*; Winkelmann, G., Ed.; CRC Press: New York, 1991; Chapter 7, pp 177–233.
(13) van der Helm, D.; Jalal, M. A. F.; Hossian, M. B. In *Iron Transport in Microbes, Plants, and Animals*; Winkelmann, G., van der Helm, D., Neilands, J. B., Eds.; VCH: New York, 1987; Chapter 9.
(14) Crumbliss, A. L. *Coord. Chem. Rev.* **1990**, *105*, 155.
(15) Matzanke, B. F.; Müller-Matzanke, G.; Raymond, K. N. In *Iron Carriers and Iron Proteins*; Loehr, T. M., Ed.; VCH Publishers, Inc.: New York, 1989; Chapter 1.
(16) Anderson, W. F. In *Inorganic Chemistry in Biology and Medicine*; Martell, A. E., Ed.; American Chemical Society Symposium Series; American Chemical Society: Washington, DC, 1980; Chapter 15.
(17) Martell, A. E., Anderson, W. F., Badman, D. G., Eds. *Development of Iron Chelators for Clinical Use*; Elsevier/North-Holland: New York, 1981.
(18) Pitt, C. G.; Martell, A. E. In *Inorganic Chemistry in Biology and Medicine*; Martell, A. E., Ed.; American Chemical Society Symposium Series; American Chemical Society: Washington, DC, 1980; Chapter 17.
(19) Winston, A.; Varaprasad, D. V. P. R.; Metterville, J. J.; Rosenkrantz, H. *Polym. Sci. Technol.* **1985**, *32*, 191.
(20) Ghio, A. J.; Zhang, J.; Piantadosi, C. A. *Arch. Biochem. Biophys.* **1992**, *298*, 646.
(21) Ghio, A. J.; Kennedy, T. P.; Whorton, R. A.; Crumbliss, A. L.; Hatch, G. E.; Hoidal, J. R. *Am. J. Physiol.* **1992**, *263*, L511.
(22) Hershko, C.; Gordeuk, V. R.; Thuma, P. E.; Thenacho, E. N.; Spira, D. T.; Hider, R. C.; Peto, T. E. A.; Drittenham, G. M. *J. Inorg. Biochem.* **1992**, *47*, 267.
(23) Hynes, J. B.; Hark, L. G. *J. Med. Chem.* **1972**, *15*, 1194.
(24) Kaczka, E. A.; Gitterman, C. O.; Dulaney, E. L.; Folkers, K. *Biochemistry* **1962**, *1*, 340.
(25) Rogers, H. J. In *Iron Transport in Microbes, Plants, and Animals*; Winkelmann, G., van der Helm, D., Nielands, J. B., Eds.; VCH Publishers: New York, 1987; Chapter 13, pp 223–233.
(26) Fish, L. L.; Crumbliss, A. L. *Inorg. Chem.* **1985**, *24*, 2198.
(27) Brown, D. A.; Glass, W. K.; Mageswaran, R.; Girmay, B. *Magn. Reson. Chem.* **1988**, *26*, 970.

0020-1669/94/1333-4077$04.50/0

stabilization of **Ib** by the R_N substituent will lead to more basic character at the carbonyl oxygen. This is manifested in the dissociation rates of a series mono(hydroxamato)iron(III) complexes,[7,8,26] including NMHA. The complexes are thermodynamically more stable and dissociate more slowly if R_N is electron-donating, due to the higher electron density on the carbonyl group. However, this correlation has been demonstrated only for the mono complexes, where a single hydroxamate is bound to the iron. Prior to this study, dissociation kinetic data on the higher bis and tris complexes were available only for AHA,[2,3,28] and no such correlation had been demonstrated for the higher complexes.

Deferriferrioxamine B, DFB, is a naturally occurring iron chelator having three hydroxamate groups which can function as iron binding sites.[9,10,29] Since DFB is hexadentate, only one ligand is needed to complete the coordination shell of the iron. In ferrioxamine B, $FeHDFB^+$ **II**, the nitrogen atom of the hydroxamate group is, in all cases, isolated from the nearest heteroatom by at least five methylene units. The electron-donating effect of the R_N substituent in deferriferrioxamine B should be roughly equivalent to NMHA and the carbonyl groups should have about the same intrinsic basicity. Therefore, any significant difference between the stepwise dissociation rates for $FeHDFB^+$ and an isocoordinate NMHA complex should be due to effects arising from the DFB backbone and not to intrinsic differences in the affinity of the hydroxamate group for iron(III).

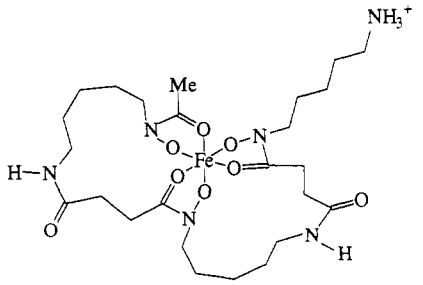

II

In an attempt to understand more fully the mechanism of iron sequestration and transport in biological systems, we report here the proton-initiated dissociation kinetics and equilibria of the three iron(III) complexes of NMHA, eqs 2–4, HL = NMHA.

$$Fe(L)_3 + H^+ \rightleftharpoons Fe(L)_2^+ + HL \qquad K_3 = k_3/k_{-3} \quad (2)$$

$$Fe(L)_2^+ + H^+ \rightleftharpoons Fe(L)^{2+} + HL \qquad K_2 = k_2/k_{-2} \quad (3)$$

$$Fe(L)^{2+} + H^+ \rightleftharpoons Fe^{3+} + HL \qquad K_1 = k_1/k_{-1} \quad (4)$$

Waters of coordination are omitted for clarity. We compare the rates and mechanism for the dissociation and formation of these complexes to acetohydroxamic acid (HL = AHA) complexes for eqs 2–4. Since NMHA should be a better model for deferriferrioxamine B than AHA, the rates and mechanism of ferrioxamine B formation and dissociation will be compared with $Fe(NMHA)_l^{3-l}$ complexes, l = 1–3.

Experimental Section

Materials and Equipment. All water used in these experiments was twice distilled, first from a solution of acidic potassium dichromate and then from basic potassium permanganate.[30] Solutions of sodium hydroxide or potassium hydroxide were prepared in CO_2-free water, standardized against potassium hydrogen phthalate to a phenolphthalein end point, and maintained under a nitrogen or argon atmosphere. Base solutions were periodically checked for CO_2 contamination by the Gran method[31] and by barium hydroxide. Stock solutions of 2.0 M sodium perchlorate were prepared from the solid hydrate (Aldrich 99.99%) and standardized by passing through a Dowex 50W-X8 strong acid cation-exchange column in H^+ form and titrating the liberated acid with standard base to a phenolphthalein end point. The 2.0 M perchloric acid stock solution was prepared from concentrated perchloric acid (Fisher 70%) and standardized to a phenolphthalein end point against standard potassium hydroxide. Ferric perchlorate stock solution was prepared from recrystallized solid ferric perchlorate hydrate and standardized for ferric ion in two ways: (1) spectrophotometrically in strong acid[32] and (2) titrimetrically by reducing with Sn(II) and titrating against primary standard potassium dichromate.[33] The acid concentration in the ferric perchlorate stock solution was determined by passing through a Dowex 50W-X8 strong acid cation-exchange column in H^+ form, titrating the liberated acid, and correcting for ferric ion.

Volumetric glassware and pipet equipment were calibrated gravimetrically before use. All pH measurements were made using a Corning 250 pH/ion meter and a Corning general purpose glass pH electrode whose reference compartment was filled with 3.0 M NaCl. NMR spectra were obtained using a General Electric QE 300 spectrometer. UV/visible spectra and slow kinetics were recorded on a Hewlett-Packard 8451 diode array spectrophotometer. Rapid kinetic studies were performed using an Aminco stopped-flow mixing device equipped with a Beckman DU UV/visible monochromator for absorbance measurements, and using a PC-486-based data acquisition station from On-Line Instruments. The monochromator was calibrated using the 400-nm peak of samarium perchlorate in solution to set the wavelength scale. The linearity of the photomultiplier response was checked against the absorbance of standard $KMnO_4$ solutions.

Ligand Preparation. *N*-methylacetohydroxamic acid (*N*-methyl-*N*-hydroxyacetamide) was prepared by reacting *N*-methylhydroxylamine with ethyl acetate in basic methanol, analogous to the method of Hauser[34] for preparation of benzohydroxamic acid from hydroxylamine and ethyl benzoate. Anal. Found (calc): C, 40.4 (40.5); H, 7.9 (8.0); N, 15.7 (15.8). NMR (in DMSO-d^6): 2.10 (3H), 3.30 (3H), 10.05 (1H). IR: ν_{OH} = 3200, ν_{CO} = 1623. MS: $MH^+ = m/e$ 90. Equivalent weight [found (theor)]: 89 ± 2 (89).

Equilibrium Studies. The pK_a titration studies were performed in 2.0 M $NaClO_4$ using a water-jacket equipped sealed cell in which a slightly pressurized argon atmosphere was maintained. The argon was purified and humidified by passing through a fritted bubbler containing Fieser's solution[35] and then through a bubbler of distilled water. The temperature was maintained at 25 °C by circulating water through the outer jacket. The temperature of the analyte solution was measured directly with an internal thermometer. Standard 0.1 M CO_2-free NaOH was delivered from a Gilmont 2.5-mL microburet. Potential measurements using a glass electrode were made directly in millivolt mode. The reference electrode was filled with 3 M NaCl in place of the standard saturated KCl to avoid problems with $KClO_4$ precipitation in the junction. The potential *vs* volume data were analyzed by the method of May and Williams using the program MAGEC.[36]

Meta–ligand binding constants were determined from two types of experiments. Mole-ratio data were obtained using a sealed titration cell from which solution could be cycled into a thermally controlled cuvette within the HP 8451 spectrophotometer using a peristaltic pump. The temperature of the titration cell was controlled by circulating water through the glass jacket surrounding the cell. Spectra were obtained as a function of metal-to-ligand ratio by titrating a solution of ferric perchlorate with NMHA. Acid-dependent spectra over the pH range from 2 to 10 were obtained and analyzed using the same apparatus except that the titration cell was fitted with a glass electrode for pH measurement. The pH meter and electrode were calibrated for measurement in 2.0 M $NaClO_4$ as follows: The electrode slope was determined using standard Fisher buffers of pH 4.00 and 7.00; then the intercept was set by standardizing the

(28) Kazmi, S. A.; McArdle, J. *J. Inorg. Nucl. Chem.* **1981**, *43*, 3031.
(29) Schwarzenbach, G.; Schwarzenbach, K. *Helv. Chim. Acta* **1963**, *46*, 1390.
(30) Monzyk, B. M. Ph.D. Dissertation, Duke University, 1980.
(31) Martell, A. E.; Motekaitis, R. J. *Determination and Use of Stability Constants*, 2nd ed.; VCH Publishers: New York, 1992.
(32) Bastian, R.; Weberling, R.; Palilla, F. *Anal. Chem.* **1956**, *28*, 459.
(33) Vogel, A. I. *Quantitative Inorganic Analysis Including Elementary Instrumental Analysis*, 3rd ed.; Longmans, Green and Co., Ltd.: London, 1968.
(34) Hauser, C. R.; Renfrow, W. B. *Org. Synth.* **1943**, *2*, 67.
(35) Albert, A.; Serjeant, E. P. *The Determination of Ionization Constants*, 3rd ed.; Chapman and Hall: London, 1984.
(36) May, P. M.; Williams, D. R. In *Computational Methods for the Determination of Stability Constants*; Leggett, D. J., Ed.; Plenum Press: New York, 1985; Chapter 3.

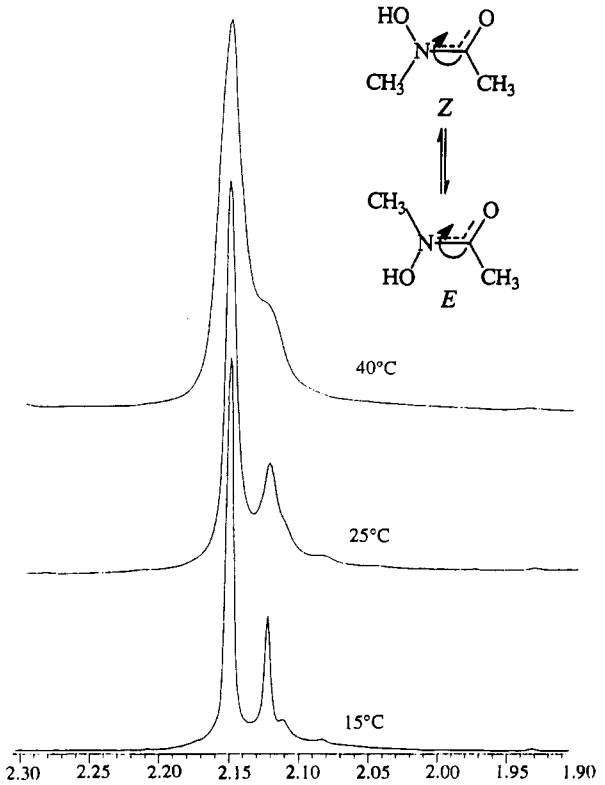

Figure 1. Temperature-dependent NMR of NMHA in the methyl region. Temperatures are approximate, ±5 °C. Spectra were measured in D_2O using a 300-MHz rf. No electrolyte was added. Units are ppm referenced against TMS in $CDCl_3$.

meter to pH 2.00 with a 0.0100 M solution of perchloric acid in 2.0 M $NaClO_4$. Acid-dependent spectra at lower pH were collected as final spectra (A_∞) after completion of kinetic runs at calculated pH values (p[H^+]) from 0 to 2.

Kinetic Studies. Dissociation kinetics were monitored by mixing equal volumes of a solution containing the Fe(NMHA)$_l^{3-l}$ complex (l = 1–3) of interest with a solution of much higher perchloric acid concentration and monitoring the absorbance between 350 and 750 nm over time at 25 °C and 2.0 M $NaClO_4$. For slow kinetics, mixing was achieved by shaking in a simple cuvette. Fast kinetic mixing was achieved in the stopped-flow unit.

Results

NMR Spectrum. The proton NMR spectrum of NMHA in D_2O shows an unequal pair of singlets at 2.13 and 2.15 ppm (3H) assigned to the *C*-methyl group, Figure 1, and another pair of unequal singlets at 3.21 and 3.26 ppm (3H) assigned to the *N*-methyl group of NMHA. In DMSO-d_6 and $CDCl_3$ an additional broad peak is observed at around 10 ppm (1H), assigned to the hydroxyl proton. The split peaks for the *N*-methyl and *C*-methyl protons are consistent with hindered rotation about the C–N bond, as has been observed for acetohydroxamic acid.[27] The rotational activation barrier results from the resonance forms **Ia,b**, in which the nitrogen lone pair is partially delocalized, giving the C–N bond partial double-bond character. At 15 °C the *C*-methyl signals sharpen and separate, but at 40 °C they coalesce into a single asymmetric peak, indicative of temperature-dependent exchange between the *Z* and *E* forms, Figure 1. Since it has been computationally determined that the hydrated *Z* form is more stable than the hydrated *E* form for formohydroxamic acid (*N*-hydroxyformamide) and acetohydroxamic acid,[37] we assign the smaller peaks to contributions from the *E* form. The R_C methyl signals are 3-Hz wide at 25 °C so that the lifetime of the shortest lived species must be at least 0.3 s and may be longer.

(37) Fitzpatrick, N. J.; Mageswaran, R. *Polyhedron* **1989**, *8*, 2255.

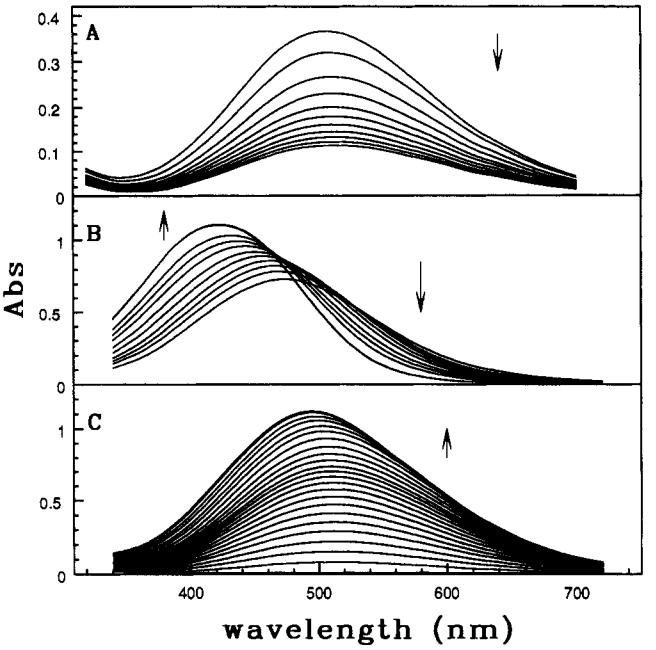

Figure 2. A: Acid-dependent spectra of Fe(NMHA)$_l^{3-l}$ complexes at various p[H^+] values, measured after kinetic runs. $[Fe^{3+}]_{tot}$ = 0.391 mM, $[NMHA]_{tot}$ = 0.781 mM, and p[H^+] = –log[H^+] = 0.00568–1.60. The arrow shows decreasing p[H^+]. B: Acid-dependent spectra of Fe(NMHA)$_l^{3-l}$ complexes at various p[H^+] values. $[Fe^{3+}]_{tot}$ = 0.410 mM, $[NMHA]_{tot}$ = 1.23 mM, and p[H^+] = 2.6–8.1. Electrode slope = 57.41, calibrated vs 0.0100 M $HClO_4$/2.0 M $NaClO_4$. Arrows show increasing p[H^+]. C: Mole-ratio spectra of Fe(NMHA)$_l^{3-l}$ complexes at various [NMHA]/[Fe^{3+}] ratios and constant [H^+]. $[Fe^{3+}]_0$ = 1.00 mM, [H^+] = 100 mM, and [NMHA]/[Fe] = 0–5.2. Species present: $Fe(NMHA)^{2+}$; $Fe(NMHA)_2^+$. The arrow shows increasing the [NMHA]/[Fe] ratio. Data for A–C are collected under conditions of 2.0 M $NaClO_4$/$HClO_4$ and 25 °C.

The peak height ratio s_Z/s_E (s_Z = height of peak assigned to the *Z* isomer, s_E = height of peak assigned to the *E* isomer) of the R_C signals is roughly equivalent to the rotational equilibrium constant K_r, assuming that the peak widths are comparable. Therefore, s_z/s_E can be used to qualitatively estimate the free energy change for the $E \rightarrow Z$ isomerization from eq 5. The ratio s_Z/s_E is 3.5, from which a free energy difference of –3.1 kJ/mol at 25 °C can be estimated for the $E \rightarrow Z$ rotation isomerization.

$$\Delta G_r = -RT \ln K_r \qquad (5)$$

Ligand Acidity. The pK_a of the NMHA ligand was determined to be 8.95(3) in 2.0 M $NaClO_4$ at 25 °C. This is consistent with hydroxamic acid acidity in general[38–41] but is higher than the previous literature value of 8.63.[38] However, in the previous study, the glass electrode used for pH measurements was calibrated directly against Fisher pH 4.00 and 7.00 buffers at 0.05 M ionic strength and then used to make measurements in 2.0 M sodium nitrate.[38] In this case, a systematic activity error as well as sodium error may be built into the pK_a value determined. In our case, the use of the MAGEC algorithm[36] for refinement of the titration data largely accounted for the H^+ activity effects incurred at the extreme ionic strength necessary for these experiments. Even though the pK_a measurements were made at pH > 7, the electrode response was linear to within less than 3% over the entire buffered pH range. Therefore, it is valid to use this pK_a value in the refinement of the iron(III) equilibria, where the electrode was calibrated below pH 7.

(38) Monzyk, B.; Crumbliss, A. L. *J. Org. Chem.* **1980**, *45*, 45.
(39) Brink, C. P.; Crumbliss, A. L. *J. Org. Chem.* **1982**, *47*, 1171.
(40) Brink, C. P.; Fish, L.; Crumbliss, A. L. *J. Org. Chem.* **1985**, *50*, 2277.
(41) Ventura, O. N.; Rama, J. B.; Turi, L.; Dannenberg, J. J. *J. Am. Chem. Soc.* **1993**, *115*, 5754.

Table 1. Equilibrium Data for $Fe(NMHA)_l^{3-l}$ and $Fe(AHA)_l^{3-l}$ (l = 1–3) Complexes[a]

L	log K_3	log K_2	log K_1
NMHA	1.06(6)	−0.9(2)	−2.75(3)
AHA	1.8[b]	−0.036[b]	−2.04[c]
K_l^{AHA}/K_l^{NMHA}	6	7	5
L	log β_3	log β_2	log β_1
NMHA	29.44(4)	21.50(3)	11.70(1)
AHA[d]	28.29	21.01	11.41

[a] K_l defined in eq 7. β_l defined in eq 6. Molar absorptivity (M^{-1} cm^{-1}) for the tris, bis, and mono NMHA complex of Fe(III) respectively, at the λ_{max} shown in parentheses: 2700 (430), 2200 (460), 1100 (510). [b] Reference 3. [c] Reference 7. [d] Reference 29.

Iron(III) Equilibria. The equilibria for the stepwise dissociation of the tris(hydroxamato)iron(III) complex are shown in eqs 2–4, where HL = NMHA. The bidentate coordination mode of NMHA is illustrated in eq 1 ($R_N = CH_3$, $R_C = CH_3$). Since each added hydroxamate group produces a characteristic spectroscopic change defined by the λ_{max} value, UV/visible spectrophotometric data provide the most convenient method for monitoring the complex equilibria and kinetics.

Three sets of data were combined in determining the K_l values: (1) spectra at constant total iron and NMHA collected from solutions after kinetic runs at 0.025–1.0 M [H^+], Figure 2A; (2) spectra at constant total iron and NMHA collected at pH 2.6–8.0, Figure 2B; (3) spectra collected at constant iron(III) and [H^+] = 0.10 M, but increasing NMHA (mole ratio), Figure 2C.

In Figure 2A, λ_{max} is a constant 510 nm at [H^+] > 0.025 M, confirming that only the $Fe(NMHA)^{2+}$ complex exists at equilibrium, even though excess ligand is present. In Figure 2B, there is no isosbestic point encompassing all of the spectra. However, at low pH there is an isosbestic point at 530 nm and at higher pH another at 470 nm, indicating that at least three complex species are present over this acidity range. Figure 2C shows the solution spectrum as a function of $[NMHA]_{tot}/[Fe^{3+}]_{tot}$ at [H^+] = 0.10 M. The shift in λ_{max} toward shorter wavelength suggests that at the higher $[NMHA]_{tot}/[Fe^{3+}]_{tot}$ ratios, a significant amount of the bis(hydroxamato)iron(III) complex is formed in addition to the mono(hydroxamato)iron(III) species.

Using the SQUAD[42] algorithm, a simultaneous global fit of *all* of the spectrophotometric data to eqs 2–4 gave an acceptable fit ($\sigma = 5 \times 10^{-3}$) and the overall logarithmic stability constants log β_l listed in Table 1. The overall stability constants, defined in eq 6,were refined by fixing the pK_a of NMHA to be 8.95. The

$$\beta_l = \frac{[FeL_l]}{[Fe][L]^l} \tag{6}$$

related stepwise pH-dependent equilibrium constants, log K_l, are defined for equilibria in eqs 2–4, as shown in eq 7. K_l values were

$$K_l = \frac{[FeL_{l-1}][HL]}{[FeL_l][H]} \tag{7}$$

computed and listed in Table 1 as well. The precision and reliability of log K_2 is somewhat lower than for the other constants but is reasonable for a bis(hydroxamato)iron(III) complex. The λ_{max} and molar absorptivity data for the three complex species were also determined from the spectrophotometric analysis by SQUAD and are listed in Table 1. All of the data in Table 1 are reasonable for (hydroxamato)iron(III) complexes in solution.

Iron(III) Dissociation Kinetics. The dissociation kinetics of the tris and bis NMHA complexes were studied at 430 nm—the λ_{max} of the tris complex—under pseudo-first-order [H^+] conditions

(42) Leggett, D. J. Stability Quotients from Absorbance Data. In *Computational Methods for the Determination of Stability Constants*; Plenum Press: New York, 1985; Chapter 6.

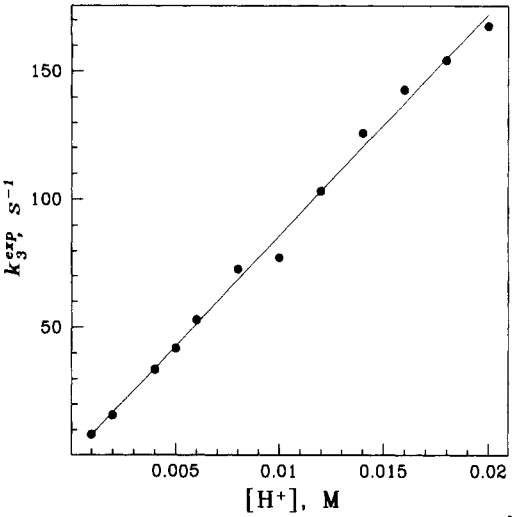

Figure 3. Acid-dependent kinetic data for the dissociation of $Fe(NMHA)_3$. $[Fe^{3+}]_{tot}$ = 0.324 mM, [NMHA] = 0.97 mM, I = 2.0 M ($NaClO_4$/$HClO_4$), and T = 25 °C. Kinetics were measured at 430 nm. Data were fit to $k_3^{exp} = a[H^+] + b$. $a = 8.6(4) \times 10^3$ M^{-1} s^{-1}, b = 0.0, and r^2 = 0.997. The uncertainty quoted is a 90% confidence limit.

and where $[Fe^{3+}]_{tot}/[NMHA]_{tot} = 1/3$. On a 1 s or less time scale, two first-order absorbance decays were observed, with decay constants k_3^{exp} and k_2^{exp} separated by at least a factor of 10 under all pH conditions employed (except for [H^+] = 0.0100 M). The faster of these two reactions, k_3^{exp}, is kinetically and spectroscopically consistant with the reaction in eq 2. Figure 3 shows a linear fit of k_3^{exp} plotted against [H^+], indicating that the reaction is first-order in proton and is irreversible under these conditions, *i.e.* the intercept is zero. Therefore, a simple rate law is proposed,

$$\frac{d[Fe(L)_3]}{dt} = -k_3[H^+][Fe(L)_3] \tag{8}$$

where $k_3^{exp} = k_3[H^+]$. The slope in Figure 3 therefore gives the microscopic rate constant k_3 to be $8.6(4) \times 10^3$ M^{-1} s^{-1}.

Under the same acidity conditions used to monitor the dissociation of the tris complex, a second slower step was observed which corresponds to the dissociation of the bis complex, $Fe(NMHA)_2^+$. The dissociation kinetics of $Fe(NMHA)_2^+$, eq 3, were studied at 500 nm under a regime in which $[Fe^{3+}]_{tot}/[NMHA]_{tot} = 1/2$ and [H^+] was varied over a much wider range. Under these conditions no tris complex, $Fe(NMHA)_3$, forms. On a 1 s or less time scale the dissociation of $Fe(NMHA)_2^+$, eq 3, is observed by its first-order absorption decay. The decay constant k_2^{exp} varies linearly with respect to [H^+], Figure 4, suggesting the simple rate law

$$\frac{d[Fe(L)^+_2]}{dt} = -k_2[H^+][Fe(L)^+_2] \tag{9}$$

where $k_2^{exp} = k_2[H^+]$. From the slope in Figure 4, we determined the microscopic rate constant k_2 to be $1.02(2) \times 10^2$ M^{-1} s^{-1}.

At the same conditions and wavelength on a time scale greater than 1 s, we observe a first-order absorbance decay associated with the dissociation of $Fe(NMHA)^{2+}$, eq 4. In this case an inverse proton dependence is observed in the plot of macroscopic rate constant k_1^{exp} against [H^+], Figure 5. This is interpreted in terms of parallel acid-dependent and acid-independent dissociation pathways for eq 4.[7,8] In other words, the reaction in eq 4 is actually a composite of the two simultaneous dissociation pathways shown in eqs 10 and 11, where waters have been omitted for clarity.

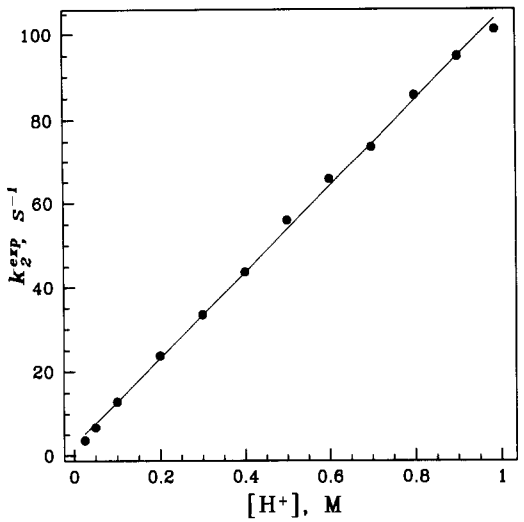

Figure 4. Acid-dependent kinetic data for the dissociation of Fe(NMHA)$_2^{2+}$. $[Fe^{3+}]_{tot}$ = 0.391 mM, $[NMHA]_{tot}$ = 0.781 mM, I = 2.0 M ($NaClO_4/HClO_4$), and T = 25 °C. Kinetics were measured at 480 nm. Data were fit to $k_2^{exp} = a[H^+] + b$. $a = 1.02(2) \times 10^2$ M^{-1} s^{-1}, b = 0.0, and r^2 = 0.999. Uncertainties quoted are 90% confidence limits.

$$FeL^{2+} + H^+ \rightleftharpoons Fe^{3+} + HL \qquad k_1, k_{-1} \tag{10}$$

$$FeL^{2+} \rightleftharpoons FeOH^{2+} + HL \qquad k_1', k_{-1}' \tag{11}$$

$$Fe^{3+} \rightleftharpoons FeOH^{2+} + H^+ \qquad \beta_H = [FeOH^{2+}][H^+]/[Fe^{3+}] \tag{12}$$

The value of β_H, the hydrolysis constant for iron(III) in 2.0 M $NaClO_4$, is 1.51×10^{-3} M[43,44] so that, below pH 1, only a small amount of hydrolyzed iron exists in solution. However, because of the higher lability of $Fe(H_2O)_5OH^{2+}$ relative to $Fe(H_2O)_6^{3+}$,[45-48] the hydrolytic second-order formation pathway, eq 11, still affects the observed relaxation kinetics. Assuming relaxation conditions hold, the rate law is[30]

$$\frac{d[FeL^{2+}]}{dt} = -\left(k_1' + k_1[H^+] + \frac{2k_{-1}'\beta_H([Fe^{3+}]_{tot} - [FeL^{2+}]_{eq})}{[H^+]}\right)[FeL^{2+}] \tag{13}$$

where k_1^{exp} is equal to the term in large parentheses and terms containing k_{-1} are negligible.[7,30] $[FeL^{2+}]_{eq}$ is the concentration of mono complex remaining after the system has reached equilibrium. By multiplying k_1^{exp} by $[H^+]$, we obtain eq 14.

$$k_1^{exp}[H^+] = k_1'[H^+] + k_1[H^+]^2 + 2k_{-1}'\beta_H([Fe^{3+}]_{tot} - [FeL^{2+}]_{eq}) \tag{14}$$

By fitting a second-order polynomial to our data for $k_1^{exp}[H^+]$ *vs* $[H^+]$ and determining the fitting parameters, as suggested by eq 14, we generate the solid line in Figure 5. Values of the microscopic rate constants—k_1 = 3.2(9) $\times 10^{-3}$ M^{-1} s^{-1} and k_1' = 7.1(3) $\times 10^{-3}$ s^{-1}—are consistent with the literature values for this system obtained at a metal-to-ligand ratio of 1:1.[7]

The last term in eq 14 arises from the reverse reaction. While eq 14 was fit by assuming this term to be constant, that is not strictly true. The spectra in Figure 2A clearly show that the concentration of Fe(NMHA)$^{2+}$ at equilibrium, $[Fe(L)^{2+}]_{eq}$, varies with pH. In addition, the large slope and relatively higher uncertainty in $[H^+]$ at the lower acid concentrations in Figure 5 do not allow for precise determination of k_{-1}' using eq 14. Consequently, k_{-1} and k_{-1}' were determined from equilibrium data and k_1 and k_1'.

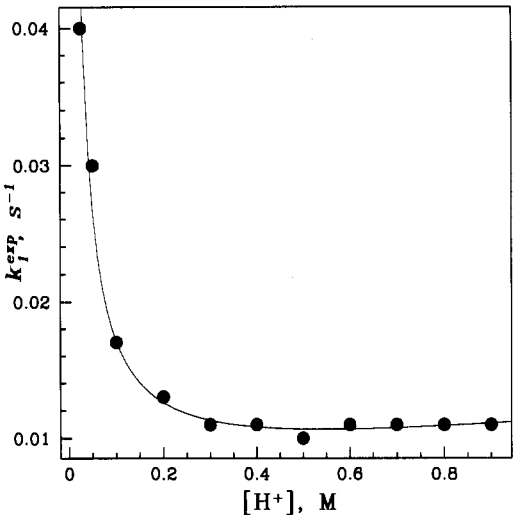

Figure 5. Acid-dependent kinetic data for the dissociation of Fe(NMHA)$^{2+}$. $[Fe^{3+}]_{tot}$ = 0.391 mM, $[NMHA]_{tot}$ = 0.781 mM, I = 2.0 M ($NaClO_4/HClO_4$), and T = 25 °C. Kinetics were measured at 480 nm. Equation 14 was fit to the data to obtain the parameters a, b, and c which were plotted as the solid line $k_1^{exp} = a + b/[H^+] + c[H^+]$, where a = 0.0071(3) s^{-1}, $b = 9.6 \times 10^{-4}$ M s^{-1}, and c = 0.0032(9) M^{-1} s^{-1}. The uncertainties quoted are 90% confidence limits.

The formation rate constants k_{-l} were computed from the relationship $K_n = k_l/k_{-l}$. The formation and dissociation rate constants are tabulated in Table 2.

Discussion

For the NMHA and AHA complexes with Fe^{3+}, Table 1 shows that complex stabilities increase when R_N is CH_3 (*vs* H), and this is interpreted in terms of delocalization of the nitrogen lone pair,[7,8,26] **Ia,b**. Greater electron-donating character at R_N stabilizes **Ib**, increasing the electron density at the carbonyl oxygen and causing it to be more basic. Crystallographic data show that the Fe–O(C) bond is shorter in a more stable ferric hydroxamate complex.[13] This indicates that the increase in stability is associated with an increase in basicity of the carbonyl oxygen and is evidence for C–N double-bond character.

The dissociation kinetic data for the iron(III) tris, bis, and mono complexes of NMHA, and for the corresponding AHA complexes, are listed in Table 2. The ratio k_l^{AHA}/k_l^{NMHA} is between 10 and 35 for all four dissociation reactions listed. This indicates a strong leaving group effect where the rate-determining step for both NMHA and AHA dissociation is similar. Furthermore, the fact that the dissociation of NMHA complexes is slower than the AHA complexes suggests that the rate-determining step in these reactions is breakage of the Fe–O(C)[7,8] bond, where electronic effects due to the R_N substituent are manifested.

Inspection of Table 1 shows that $K_l^{AHA}/K_l^{NMHA} = 6 \pm 1$ for all three steps. The following quantities from Figure 6 are defined for the formation and dissociation reactions of FeL_l (HL = AHA or NMHA):

ΔG_r = the free energy difference in the reacting species

ΔG_p = the free energy difference in the products

A constant ratio of dissociation equilibrium constants implies that

(43) Milburn, R. M.; Vosburgh, W. C. *J. Am. Chem. Soc.* **1955**, *77*, 1352.
(44) Milburn, R. M. *J. Am. Chem. Soc.* **1957**, *79*, 537.
(45) Biruš, M.; Kujundžić, N.; Pribanić, M. *Prog. React. Kin.* **1993**, *18*, 173.
(46) Swaddle, T. W.; Merbach, A. E. *Inorg. Chem.* **1981**, *20*, 4212.
(47) Grant, M.; Jordan, R. B. *Inorg. Chem.* **1981**, *20*, 55.
(48) Dodgen, H. W.; Liu, G.; Hunt, J. P. *Inorg. Chem.* **1981**, *20*, 1002.

Table 2. Microscopic Rate Constants for $Fe(NMHA)_l^{3-l}$ and $Fe(AHA)_l^{3-l}$ (l = 1–3) Complex Formation and Dissociation[a]

L	$10^{-3}\,k_3$	$10^{-2}\,k_{-3}$	$10^{-2}\,k_2$	$10^{-2}\,k_{-2}$	$10^{3}\,k_1$	k_{-1}	$10^{3}\,k'_1$	$10^{-3}\,k'_{-1}$
NMHA	8.6(4)	7.5(4)[b]	1.02(2)	8.1(7)[b]	3.2(3)[f]	1.80(3)[b,f]	7.1(3)[f]	2.65(1)[c,f]
AHA	100[d]	17[d]	14[d]	16[d]	110[e]	1.2[e]	80[e]	2.0[e]

[a] All rate constants in units of $M^{-1}\,s^{-1}$ except k'_1, which is s^{-1}. All data in 2.0 M $NaClO_4/HClO_4$ at 25 °C. Uncertainties in parentheses are 90% confidence limits. [b] Calculated from the equilibrium constant. [c] Calculated from the equilibrium constant and Fe(III) hydrolysis constant β_H. [d] Reference 3. [e] Reference 7. [f] Compares favorably with previous literature data.[7]

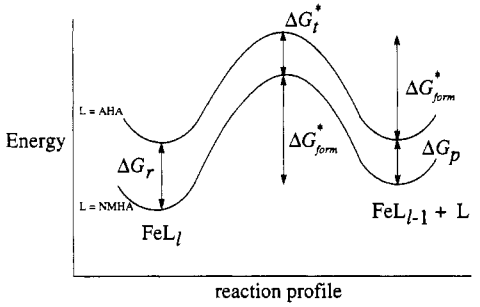

Figure 6. General free energy profile for ferric hydroxamate dissociation reaction illustrating variations in ground-state and transition-state energies. The absolute energies shown for $Fe(NMHA)_l$ and $Fe(AHA)_l$ systems are arbitrary.

$$\Delta G_r - \Delta G_p = C \qquad (15)$$

where C is a constant. Since $K^{AHA} > K^{NMHA}$ for all three steps, $\Delta G_r > \Delta G_p$ for all l = 1–3. That C is constant is not surprising since an examination of the total reaction profile for each dissociation step reveals that all three steps differ only by the presence one or two additional hydroxamate ligands in the inner coordination shell. These observations, however, say nothing about the actual values of ΔG_r and ΔG_p.

Another piece of relevant information comes from the fact that for all three dissociation steps, the reverse (or formation) reaction occurs at nearly the same rate for AHA and NMHA ligands, Table 2. This means that ligand-dependent variations in the transition-state energy closely parallel ligand-dependent variations in the ground-state products of Figure 6, *i.e.*

$$\Delta G_t^{\ddagger} \approx \Delta G_p \qquad (16)$$

The implication is that there is a late transition state for the dissociation reaction, where structural variations in the transition state parallel structural variations in the product ground state. A late transition state means that the leaving group has largely dissociated from the metal center so that the transition state has character more like the dissociated products than like the undissociated reactants.

A third piece of information comes from a consideration of the energetics of the dissociation process. Figure 7 shows the dissociation rate constant, ln k_{diss}, plotted against the dissociation equilibrium constant, ln K_{diss}, for each of the three dissociation steps of $Fe(NMHA)_l^{3-l}$ and $Fe(AHA)_l^{3-l}$. The theoretical reason for plotting the dissociation data in this way stems from eq 16, which itself is a result of the fact that, for a given set of reaction profiles as shown in Figure 6, $\Delta G^{\ddagger}_{form}$ is independent of entering group L. Since

$$\ln K_{diss} = \ln k_{diss} - \ln k_{form} \qquad (17)$$

and ln k_{form} is constant for a given l, a theoretical linear relationship exists between ln K_{diss} and ln k_{diss}, when eq 15 holds. The magnitude of the activation barrier for the dissociation process is highly correlated with the relative ground-state energy of the reactant. Variations in dissociation rate must be due almost entirely to ligand-dependent variations in the energy of the reactants, since there is essentially no ligand dependence in the formation direction. This is further evidence for a late transition

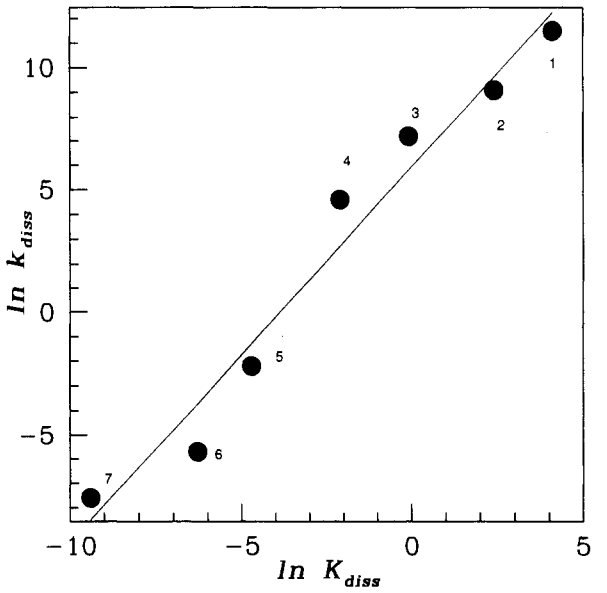

Figure 7. Plot of ln k_{diss} *vs* ln K_{diss} for iron(III) dissociation reactions with NMHA, AHA, and H_3DFB ligands. All data were measured in aqueous 2.0 M $NaClO_4/HClO_4$ at 25 °C. Data are from Tables 1 and 2 and from the literature as noted. Slope = 1.5(4), intercept = 6(2), and r^2 = 0.98. The uncertainties quoted are 90% confidence limits. Key: (1)[3] $Fe(AHA)_3$ (2) $Fe(NMHA)_3$; (3)[3] $Fe(AHA)_2^+$; (4) $Fe(NMHA)_2^+$; (5)[3] $Fe(AHA)^{2+}$; (6) $Fe(NMHA)^{2+}$; (7)[10] bidentate ferrioxamine B (FeH_3DFB^{3+}).

state in the dissociation of ferric hydroxamates, where the ligand plays a minimal role in the transition-state structure and energetics.

In the ideal circumstance where there is complete correlation between the activation barrier and the reactant ground-state stability, Figure 7 should have a slope of unity as suggested by eq 17. The actual slope in Figure 7 is 1.5(4). It may be that the small data set and fairly large uncertainty mask a unit slope or that the correlation between dissociation rate and ground-state energetics is not complete. An incomplete correlation suggests at least *some* participation by the leaving group in the transition state, though the reasonably linear plot in Figure 7 still suggests that the leaving group dissociates early in the reaction profile.

The fact that dissociation data for all three steps in the dissociation of $Fe(NMHA)_l^{3-l}$ and $Fe(AHA)_l^{3-l}$ fall on the same line in Figure 7 suggests that the transition states are all similar and that the dissociation mechanisms are also similar. Since it has been fairly well established that Fe–O(C) bond breakage is the rate-limiting step in the dissociation of the mono complex,[7,8,26] Fe–O(C) bond breakage must also be the rate-limiting step in the bis and tris dissociation reactions as well to maintain mechanistic similarity.

On the basis of these observations, we can discount a completely associative mode of activation as being inconsistent with a pronounced and systematic leaving group effect for the dissociation reactions and the lack of entering group effect in the formation reactions. However, negative $\Delta S^{\ddagger}$ values for the formation and dissociation of mono(hydroxamato)iron(III) complexes[7,8,26]—including NMHA and AHA ligands[7]—and the nonunit slope in Figure 7 suggest at least some participation by the ligand in the transition state when the active iron species is $Fe(OH_2)_6^{3+}$. On the basis of the comparison with water exchange data at Fe-

Scheme 1. General Mechanism of (Hydroxamato)iron(III) Dissociation (L = H_2O or Hydroxamate Oxygen and Charges Omitted for Clarity)

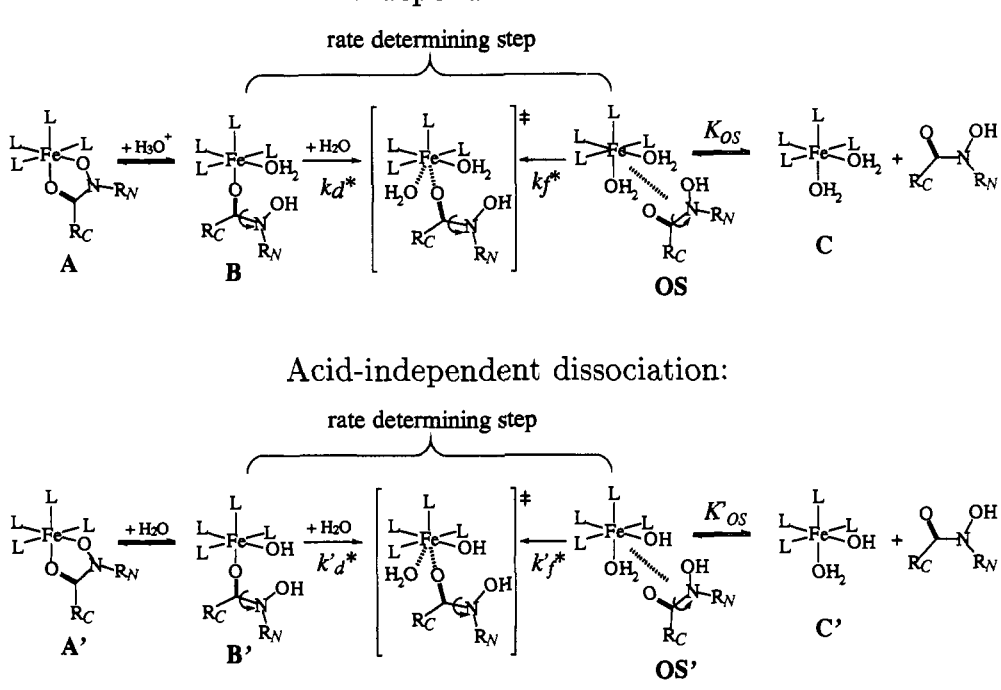

$(OH_2)_6^{3+}$ and $Fe(OH_2)_5OH^{2+}$,[46-48] an I_a activation mode has been proposed for hydroxamate exchange at $Fe(OH_2)_6^{3+}$.[7,8]

An unambiguous assignment of the role of water exchange in the higher complex reactions cannot be made since water exchange data are not available for higher hydroxamate complexes. However, the fact that the dissociation of the bis and tris complexes are collinear in Figure 7 suggests that, by analogy with the mono system, we tentatively assign an I_a mechanism to the dissociation of the bis and tris complexes. However, since water exchange rates increase 3 orders of magnitude when a hydroxide ligand is present in the inner coordination shell of iron(III),[46-48] we may expect a similar increase in water lability when a hydroxamate ligand binds to iron(III). This may facilitate an increase in ligand exchange rate as well as a shift to more dissociative character in the interchange reaction as the number of hydroxamates in the inner coordination shell increases. In fact, pressure studies on the bis- and tris(acetohydroxamic acid) complexes of iron(III) do show volumes of activation less negative than the mono complex, suggesting some shift toward more dissociative character.[2]

The NMHA data combined with the data for other model hydroxamic acids are consistent with the mechanism in Scheme 1. Though subtle differences in the degree of Fe–O(C) bond formation in the transition state may exist for the mono, bis, or tris complexes—as mentioned previously—Scheme 1 is otherwise general. The initial step in the formation direction involves an outer-sphere encounter complex **OS**. The formation of the outer-sphere complex is supported by pressure studies on $Fe(AHA)_l^{3-l}$ complexes, where the small volumes of activation suggest an interchange mechanism.[2] **OS** may involve some hydrogen-bonding interaction with the water in the inner coordination shell.[7,8] Then a dissociative replacement of a water ligand by the carbonyl oxygen occurs in the rate-determining step to yield the quasi-stable intermediate **B**, which rapidly undergoes ring closure with loss of hydronium ion to give the complex **A**.

The acid-independent path is experimentally observed only for the formation of the mono complex, due to the lower acidity of waters in the coordination shell of higher (hydroxamato)iron(III) complexes. The transition state for this path involves one less proton than for the acid-dependent pathway. Scheme 1 shows the proton having been removed from an inner coordination shell water since it should be more acidic than the OH proton on the hydroxamic acid. The presence of the hydroxide has a labilizing effect on the metal–ligand bonds, allowing for greater dissociative character. Hydroxide may also allow for somewhat stronger binding in **OS'** compared to **OS**, due to H-bonding between the hydroxamic acid and the hydroxide ligand. The final step, **B'** → **A'**, then involves loss of water instead of hydronium.

The actual second-order rate constant k for the formation of **A** or **A'** is related to k^* by eq 18 (where $k^* = k^*_f$ or k'^*_f),

$$k = K_{OS}Sk^* \qquad (18)$$

according to an Eigen–Wilkins mechanism.[49] The factor S is introduced to correct for the composition of the outer solvation shell.[8] Assuming 12 water molecules can occupy the outer shell and that the hydroxamate ligand can replace two of these, $S = {}^1/_6$. Mechanistic trends for water exchange at $Fe(OH_2)_6^{3+}$ and $Fe(OH_2)_5OH^{2+}$ hold for ligand substitution by hydroxamate ligands as well.[2,7,8,26,45-47] Given the dissociative nature of the rate-determining step, the rate constant k^* is, in theory, equivalent to the water exchange rate at the metal center.[8,12,45,49] We can insert water exchange data[47] and $Fe(NMHA)^{2+}$ formation data into eq 18 to estimate $K_{OS} = 0.07\ M^{-1}$ and $K'_{OS} = 0.13\ M^{-1}$ for the acid-dependent and acid-independent dissociation paths, respectively, in Scheme 1. Since the ligand is uncharged, it will have no particular affinity for higher charged metal ions. It is not surprising, then, that K_{OS} and K'_{OS} are nearly equal. Indeed, the fact that the estimated outer-sphere formation constants for $Fe(OH_2)_6^{3+}$ and $Fe(OH_2)_5OH^{2+}$ are in such close agreement is some validation of eq 18. Therefore, the actual ligand substitution process appears to be dominated by factors related to water exchange, and mechanistic assignments for hydroxamate substitution based on water exchange data are applicable. Unfortunately, no water exchange data are available for the higher hydroxamate complexes that would allow extension of this analysis to formation of bis- and tris(hydroxamato)iron(III) complexes.

It is worthwhile to consider the effect of C–N rotation on the dissociation mechanism. In the case of NMHA, the C–N rotation

(49) Eigen, M.; Wilkins, R. G. *Adv. Chem. Ser.* **1965**, *No. 49*, 55.

Scheme 2. Dissociation Mechanism of $Fe(NMHA)_l^{3-l}$ and Ferrioxamine B

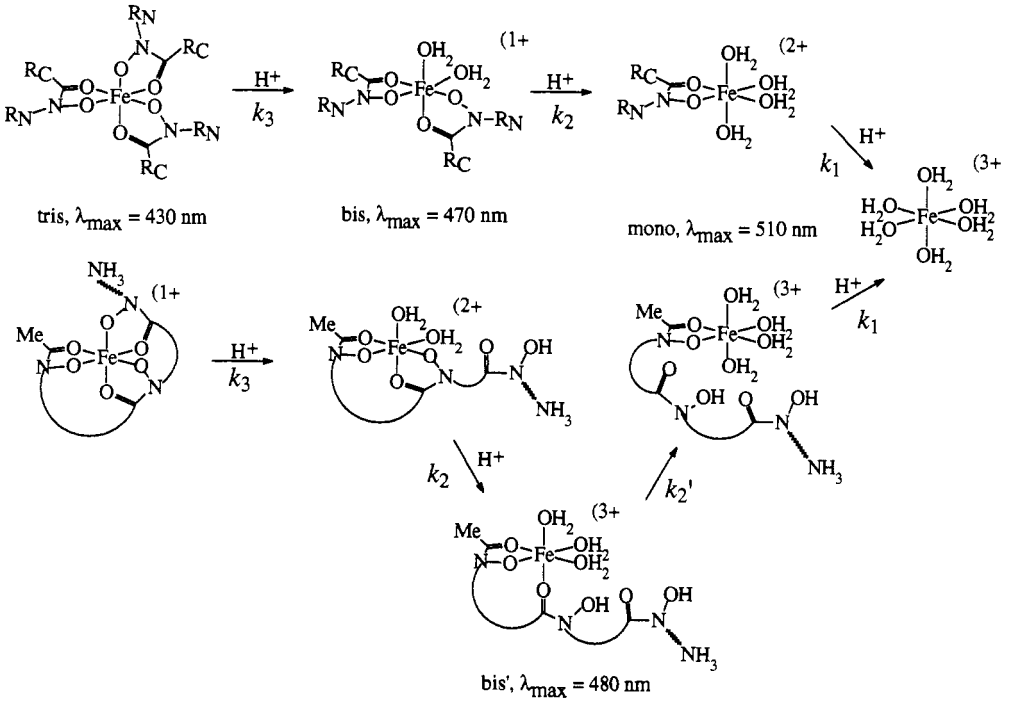

Table 3. Dissociation Kinetic Data for Ferrioxamine B[a]

ref	k_3	k_2	k'_2	k_1	k'_1
9	2.9×10^{2} [b]	1.4×10^{1} [b]	1.8×10^{-1} [b]	1.9×10^{-3} [c]	2.1×10^{-3} [b]
10	3.8×10^{2} [c]	0.99×10^{1} [b]	2.3×10^{-2} [c]	5×10^{-4} [c]	9.3×10^{-4} [b]

[a] All data at 2.0 M $NaClO_4/HClO_4$ and 25 °C. [b] s^{-1}. [c] M^{-1} s^{-1}.

rate has been shown to be on the order of 3 s^{-1} or slower at 25 °C, based on qualitative inspection of the NMR spectrum. This is slower than the ligand exchange reaction at the tris complex, so that, in the dissociation of the tris complex, the hydroxamate group will not be able to rotate into the *E* conformation on the time scale of the chemical reaction. The rate of rotation is likely to be considerably faster than ligand exchange involving the mono complex, and so the *rate* of rotation will not explicitly affect the dissociation mechanism but will only modify its overall rate by the factor K_r. On the other hand, the ligand exchange processes involving the bis complex occur on a time scale that may be comparable to the rate of rotation, making detection of multiple kinetic steps more likely. Though this is not observed in the case where HL = NMHA, C–N bond rotation may explain an anomaly observed in the dissociation mechanism of the ferrioxamine B complex, **II**.

The dissociation mechanism of the open-chain trihydroxamate siderophore ferrioxamine B ($FeHDFB^+$) is illustrated in Scheme 2, in parallel with the analogous dissociation reaction of $Fe(NMHA)_3$. Two independent research groups[9,10] have found that the dissociation of $FeHDFB^+$ occurs in four steps, Table 3, instead of three as expected on the basis of the dissociation of the model tris(hydroxamato)iron(III) complexes, Table 2. The discrepancy in $FeHDFB^+$ appears to involve the bis → mono reaction, Scheme 2, where two steps are observed instead of the expected one. The spectrophotometric evidence indicates that both steps involve some dechelation at the iron center. The bis → mono reaction in $FeHDFB^+$ dissociation is where the size effects from both the R_N and R_C substituents are maximized and where we might expect the rotation rate about C–N to be slowest. Furthermore, the large R_N and R_C substituents may stabilize the E conformation of the hydroxamate group somewhat, making it more difficult for the C–N bond to rotate into a position favorable for bidentate iron binding. These steric factors may be responsible for observation of a half-bonded intermediate, **bis'**,[9] Scheme 2, analogous in many ways to **B**, Scheme 1. This is consistent with the fact that only one step is observed for the dissociation of the first or last hydroxamates from $FeHDFB^+$, where steric effects should be smaller and the rate of rotation about C–N more rapid. This effect has not been observed in the case of model mono(hydroxamato)iron(III) complexes, where C–N rotation would be expected to be more rapid.

The deferriferrioxamine B (H_4DFB^+) ligand, in **II**, has alkyl groups at R_N and R_C. The oxime nitrogen in H_4DFB^+ is isolated from the nearest heteroatom by 5 methylene units. This means that the degree of double-bond character in the C–N bond, and the basicity of the carbonyl oxygen, should be about the same as for NMHA. Therefore, large differences in the kinetics of $FeHDFB^+$ and $Fe(NMHA)_l^{3-l}$ complexes must be due to secondary effects arising from the backbone and not from intrinsic reactivity differences between the two ligands. The literature data available for the dissociation of $FeHDFB^+$ [9,10] are shown in Table 3. The only steps that will be directly comparable to $Fe(NMHA)_l^{3-l}$ dissociation are k_3, k_1, and k'_1. The middle steps k_2 and k'_2 are mechanistically different as discussed above, and there is still some uncertainty in the literature as to the magnitudes and interpretation of those data.[9,10]

Two possible explanations exist for the fact that the tris → bis reaction is 25 times as fast in $Fe(NMHA)_3$ as in $FeHDFB^+$. One is that the extra positive charge on the $FeHDFB^+$ complex, Scheme 2, due to the protonated amine electrostatically repels the incoming proton necessary for dissociation. The second is that there is a large solvent rearrangement factor to account for in dissociating the hydroxamate group of $FeHDFB^+$ due to the chelate arm connecting one hydroxamate to another. The solvent cage resists the motion of the arm as it tries to dissociate from the iron, increasing the activation barrier. Both of these explanations are consistent with the fact that for the comparable dissociation of the bidentate $Fe(NMHA)^{2+}$ and bidentate bound ferrioxamine B, FeH_3DFB^{3+}, k_1^{NMHA}/k_1^{DFB} and k_1^{NMHA}/k_1^{DFB} are both approximately less than 5, compared to the factor of 25 difference in k_3 values for dissociation of the tris complexes. In the final dissociation step, the positive charge on the protonated amine is far from the metal site[9] and may not electrostatically affect the approach of the proton to this point, especially in high ionic strength media. In the mono dissociation reaction, Scheme 2,

there also need not be a large rearrangement of the ligand to remove the iron, making dissociation of the bidentate form of ferrioxamine B more like dissociation of $Fe(NMHA)^{2+}$.

Summary and Conclusions

The iron equilibria and dissociation kinetics were measured for the $Fe(NMHA)_l^{3-l}$ complexes where $l = 1-3$. The dissociation rates when $l = 1$ compare favorably with previous literature reports on dissociation of the mono complex. This work is the first report on the dissociation kinetics of the higher ($l = 2, 3$) complexes of NMHA with iron(III). Structural effects on the dissociation rate were discussed and related to analogous mechanistic steps in the dissociation of $Fe(AHA)_l^{3-l}$ complexes. On the basis of the linear free energy correlation in Figure 7, the mechanism and mode of activation in $Fe(NMHA)_l^{3-l}$ dissociation is proposed to be similar for all three dissociation steps. The mechanism for NMHA dissociation is compared to analogous processes in the dissociation of the naturally occurring siderophore system ferrioxamine B. The fundamental mechanistic difference is in the dissociation of the tetradentate form of ferrioxamine B, which proceeds *via* a two-step process, whereas the dissociation of $Fe(NMHA)_2^+$ to give $Fe(NMHA)^{2+}$ occurs in a single observable step, eq 3. C–N rotation in ferrioxamine B and NMHA is offered as a possible reason for this mechanistic discrepancy. Since the ligand electronic factors affecting the dissociation of $Fe(NMHA)_l^{3-l}$ and ferrioxamine B are similar, the consistently slower rates for the stepwise dissociation of ferrioxamine B are ascribed to secondary structural factors related to the ligand, including size and overall charge of the iron complex. Both of these hypotheses can be supported by the available data.

Acknowledgment. Financial support for this research from the American Chemical Society Petroleum Research Fund and the National Science Foundation (CHE-9113199) is gratefully acknowledged.